 CMC, vol.37, no.2, pp.77-96, 2013

An Improved Concrete Damage Model for Impact Analysis of Concrete Structural Components by using Finite Element Method

A. Ramachandra Murthy[1], G.S. Palani[1], Smitha Gopinath[1], V. Ramesh Kumar[1] and Nagesh R. Iyer[1]

Abstract: This paper presents the development of an improved concrete damage model for projectile impact on concrete structural components. The improvement is in terms of reduction of input material parameters for nonlinear transient dynamic impact analysis by employing concrete damage model. The experimental data such as pressure vs volumetric strain, triaxial compression failure and pressure vs stress difference have been used for evaluation of the important parameters of concrete damage model. Various contact algorithms have been outlined briefly to model the interface between the projectile and target. The nonlinear explicit transient dynamic analysis has been carried out by using finite element method to compute the responses. It is observed that the computed penetration depth obtained in the present study is in good agreement with those values of corresponding experimental studies and LS-DYNA.

Keywords: Impact Analysis, Concrete Damage Model, Nonlinear Transient Dynamic Analysis, Finite Element Method.

1 Introduction

Concrete is a widely used material in civil and defense constructions. Potential missiles/projectiles include kinetic munitions, vehicle and aircraft crashes, fragments generated by military and terrorist bombing, fragments generated by accidental explosions and other events (e.g. failure of a pressurized vessel, failure of a turbine blade or other high-speed rotating machines), flying objects due to natural forces (tornados, volcanoes, meteoroids), etc. These projectiles vary broadly in their shapes and sizes, impact velocities, hardness, rigidities, impact attitude (i.e. obliquity, yaw, tumbling, etc.) and produce a wide spectrum of damage in the target.

[1] CSIR-Structural Engineering Research Centre, CSIR Campus, Taramani, Chennai-113.

Numerous studies were carried out in the last 15 years for the development and improvement of the macro-scale concrete models for high-pressure applications [Govindjee et al. (1995); Malvar et al. (1997); Govindjee et al. (1994); Hentz et al. (2004); Yonten et al. (2005); Farnam et al. (2010); Rama Chandra Murthy et al. (2008)]. Various material models were proposed from relatively simple to more sophisticated ones. Their capabilities in describing the actual nonlinear behaviour of concrete under different loading conditions vary. Besides, because of the general complexity of the models, the determination of the model parameters (i.e., the model parameterization) also plays an important role in the actual performance of these models. This requires a sufficient understanding of the material formulation and the associated considerations. There are three important methods for studying local effects [Rama Chandra Murthy et al. (2009)] on a concrete target arising from projectile impact, namely experimental, analytical and numerical methods. Experimental data are always of importance extending the understanding of impact phenomena and for validating analytical and numerical models. Empirical formulae based on experimental data are also important due to the simplified expressions to represent complexity of the phenomena. Several design codes employ empirical formulae for the design of protective barriers. Simple and accurate analytical models can be developed when the underpinning mechanics of the local effects of the missile impact are understood. This approach offers the most efficient and economic way of predicting impact effects and helps to extend the range of validity of experimentally based empirical formulae. With the rapid developments of computational tools, computational mechanics, material constitutive models and the numerical simulation of local projectile impact effects becomes more reliable and economic. A number of commercial hydro codes such as AUTODYN (2001) and LS-DYNA (2003) are available for the general simulation of structural nonlinear dynamic responses. However, such simulations can produce reliable results for concrete structures, only if a material model capable of representing the essential mechanical processes of the material under varying stress and loading rate conditions is available. It is observed from literature [Govindjee et al. (1995); Malvar et al. (1997); Govindjee et al. (1994); Hentz et al. (2004); Yonten et al. (2005); Farnam et al. (2010); Rama Chandra Murthy et al. (2008); Rama Chandra Murthy et al. (2009); Hu et al. (2012)] that various material models such as soil/crushable foam model, isotropic elastic-plastic with oriented cracks model, kinematic hardening cap model, soil/concrete model, brittle damage model, JH model and Gebbeken-Ruppert model, Johnson and Holmquist concrete model, concrete damage model etc., are generally used for concrete to represent the impact phenomena. The concrete damage model is widely employed for simulation of nonlinear behaviour of concrete. This model requires many input parameters, which are to be obtained from experiments.

The objective of this paper is to present the details of an improved concrete damage model for projectile impact analysis and to conduct nonlinear transient dynamic analysis of concrete structural components. Brief discussion on concrete damage model, various contact algorithms and procedure to conduct nonlinear explicit transient dynamic analysis is provided.

2 Concrete Damage Model

The concrete damage model was first developed for DYNA3D [Govindjee et al. (1995); Malvar et al. (1997); Farnam et al. (2010)]. The concrete damage model uses three independent strength surfaces, namely, an initial yield surface, a maximum failure surface and a residual surface, with consideration of all the three stress invariants (I_1, J_2 and J_3). The strength surfaces are uniformly expressed as:

$$\Delta\sigma = \sqrt{3J_2} = f(p, J_2, J_3) \tag{1}$$

where $\Delta\sigma$ and p denote, respectively, the principal stress difference and pressure, and

$$f(p, J_2, J_3) = \Delta\sigma^c * r' \tag{2}$$

where $\Delta\sigma^c$ represents the compressive meridian and r' can be calculated by using the formula given below.

$$r' = \frac{r}{r_c} = \frac{2(1-\psi^2)\cos\theta + (2\psi-1)\sqrt{4(1-\psi^2)\cos^2\theta + 5\psi^2 - 4\psi}}{4(1-\psi^2)\cos^2\theta + (1-2\psi)^2} \tag{3}$$

where $\psi = r_t/r_c$(refer to Figure 1). The Lode angle, θ is a function of the second and third deviatoric stress invariant and can be obtained by either of the following two equations:

$$\cos\theta = \frac{\sqrt{3}}{2}\frac{s_1}{\sqrt{J_2}} \text{ or } \cos 3\theta = \frac{3\sqrt{3}}{2}\frac{J_3}{J_2^{3/2}} \tag{4}$$

In Eq.4, s_1 is the s_1 is first principal deviatoric stress.

The compressive meridians of the initial yield surface $\Delta\sigma_y^c$, the maximum failure surface $\Delta\sigma_m^c$ and the residual surface $\Delta\sigma_r^c$ are defined independently as [Malvar et al. (1997)]:

$$\Delta\sigma_y^c = a_{0y} + \frac{p}{a_{1y} + a_{2y}p} \tag{5}$$

$$\Delta\sigma_m^c = a_0 + \frac{p}{a_1 + a_2 p} \tag{6}$$

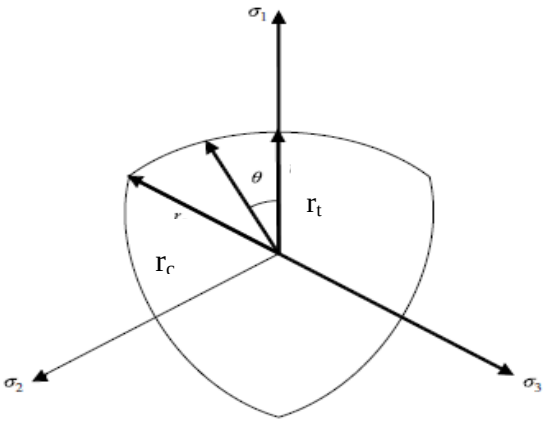

Figure 1: Typical deviatoric cross-section of strength surface.

$$\Delta\sigma_r^c = \frac{p}{a_{1f} + a_{2f} p} \tag{7}$$

The eight free parameters, namely, a_{0y}, a_{1y}, a_{2y}, a_0, a_1, a_2, a_{1f}, and a_{2f} are to be determined from experimental data.

With the specification of the three strength surfaces, the loading surfaces representing strain hardening after yield are defined as:

$$\Delta\sigma_L = \eta\Delta\sigma_m + (1-\eta)\Delta\sigma_y \tag{8}$$

The post-failure surfaces, denoted by$\Delta\sigma_{pf}$, are defined in a similar way by interpolating between the maximum failure surface $\Delta\sigma_m$ and the residual surface$\Delta\sigma_r$:

$$\Delta\sigma_{pf} = \eta\Delta\sigma_m + (1-\eta)\Delta\sigma_r \tag{9}$$

The variable η in Eqs. (8) and (9) is called the yield scale factor, which is determined by a damage functionλ:

$$\lambda = \begin{cases} \int_0^{\bar{\varepsilon}_p} \frac{d\bar{\varepsilon}_p}{[1+p/f_t]^{b1}} & p \geq 0 \\ \int_0^{\bar{\varepsilon}_p} \frac{d\bar{\varepsilon}_p}{[1+p/f_t]^{b2}} & p < 0 \end{cases} \tag{10}$$

where f_t is the quasi-static concrete tensile strength, $d\bar{\varepsilon}_p$ is effective plastic strain increment and $d\bar{\varepsilon}_p = \sqrt{\frac{2}{3} d\varepsilon_{ij}^p d\varepsilon_{ij}^p}$ with $d\varepsilon_{ij}^p$ being the plastic strain increment tensor.

It is to be noted that the damage function has different definitions for compression $(p \geq 0)$ and tension $(p < 0)$ to account for different damage evolution of concrete

in tension and compression. The evolution of the yield scale factor η follows a general trend that it varies from "0" to "1" when the stress state advances from the initial yield surface to the maximum failure surface and changes from "1" back to "0", when the stress softens from the failure surface to the residual surface. Further, from Eq.8, it can be noted that η varies from 0 to 1 depending on the accumulated effective plastic strain parameter λ. After reaching the maximum surface the current failure surface is interpolated between the maximum and the residual as shown in Eq.9. The function $\eta(\lambda)$ is input as a series of $(\eta\ ,\lambda)$ pairs. This function (Eq.10) begin at 0 at $\lambda = 0$, increase to 1 at some value $\lambda = \lambda_m$ and then decrease to 0 at some larger value of λ.

3 An Improved Concrete Damage Model

The original concrete damage material model decouples the volumetric and deviatoric responses. An equation of state gives the pressure as a function of current and previous minimum (most compressive) volumetric strain. The volumetric response is easily captured via a tabulated input data such as the one in equation of state. However, the deviatoric response present some shortcomings, which are addressed with modifications. Due to the decoupling of volumetric and deviatoric responses, this model has the limitation of not incorporating shear dilation, which is generally observed with concrete. For the case of significant structural lateral restraints and low damage levels, this will result in responses softer than expected. During initial loading or reloading, the deviatoric stresses remain elastic until the stress point reaches the initial yield surface. The deviatoric stresses can then increase further until the maximum yield surface is reached. Beyond this stage, the response can be perfectly plastic or soften to the residual yield surface (see Figure 2). Whenever the stress point is on the yield surface and the stress increment corresponds to loading on that surface, plastic flow occurs in accordance with a Prandtl-Reuss (volume preserving) flow rule, which is represented implemented by the well known "radial return" algorithm. The model also incorporates a tensile cut-off and a pressure cut-off, which are detailed in the following.

It is well known that the concrete damage model requires eight constants, namely, a_{0y}, a_{1y}, a_{2y}, a_0, a_1, a_2, a_{1f}, and a_{2f}, which are generally obtained from appropriate experimental data. In addition, an-equation-of-state is to be defined for this model. Tabulated values consisting of pressure versus volume is to be given as input to define equation-of-state, which is generally obtained from the experiments.

Schwer and Malvar (2005) characterized 45.6 MPa unconfined compression strength concrete, which is commonly used as the 'standard concrete' in many numerical simulations. The experimental data can be used as input for numerical simulation, which will reduce the evaluation of constants. The following modifications are

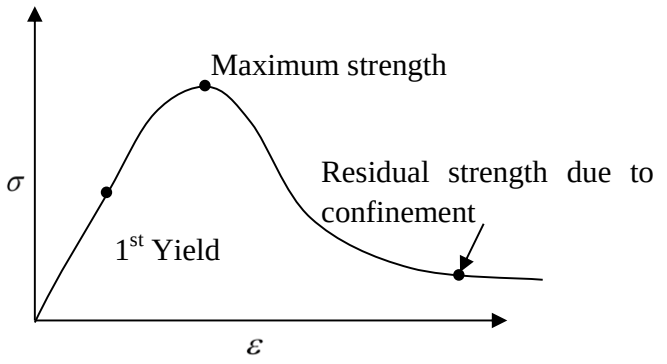

Figure 2: Three failure surfaces .

carried out to the existing concrete damage model:

- Generalization of equation-of-state
- Evaluation of constants, a_o, a_1 and a_2 based on triaxial compression failure test data
- Determination of yield surface parameters, a_{0y}, a_{1y} and a_{2y} based on triaxial failure surface
- Evaluation of residual failure surface constants, a_{1f} and a_{2f} from the triaxial compression test
- Computation of damage scaling factor, b_1, b_2 and b_3 based on uniaxial and triaxial tensile path

3.1 Generalization of equation-of-state

Figure 3 shows the pressure versus volume strain response for the 45.6 MPa concrete under isotropic compression. This laboratory test was performed on right circular cylinders of concrete, where loads (pressures) are applied independently to the top and lateral surfaces the axial and lateral strains were measured on the outer surface of the specimen. For this isotropic (hydrostatic) compression test, the applied axial and lateral pressures are equal. The pressure versus volume strain response has three general phase:

1. An initial elastic phase as low pressure and volume strains; the slope of this portion of the response curve is the elastic bulk modulus.

2. A large amount of straining as the void in the concrete are collapsed, while the pressure increases less dramatically (lower slope).

3. The final phase of compaction is reached, when all the voids are collapsed and the material response stiffens.

4. The slope of unloading path shown in Figure 3 provides an estimate of the bulk modulus of the fully compacted concrete.

Table 1 shows the data of pressure vs volumetric strain for 45.6 MPa concrete [Schwer and Malvar (2005)].

Table 1: Pressure vs Volumetric strain data.

Pressure	Volumetric strain	Pressure	Volumetric strain	Pressure	Volumetric strain
1.16248	7.57E-05	411.611	0.045375	224	0.047136
18.5027	0.001735	449.668	0.049521	195.193	0.04509
60.3243	0.004609	491.171	0.054118	147.532	0.041987
109.024	0.008462	528.066	0.058189	102.417	0.037837
137.795	0.011928	557.958	0.061955	67.8194	0.034068
195.268	0.019233	483.157	0.059285	45.9539	0.031431
233.256	0.023754	422.501	0.056474	25.3202	0.028496
286.079	0.030757	344.337	0.052902	13.9447	0.02639
325.187	0.035578	301.145	0.051077	9.65501	0.024139
360.919	0.039572	257	0.0493	0.784643	0.02121

3.2 Evaluation of constants, a_0, a_1 and a_2

Constants, a_0, a_1 and a_2 are obtained by using the test data of triaxial compression failure surface [Schwer and Malvar (2005)]. It is well known that the concrete damage model uses a three parameter function to represent the variation of compressive shear strength with mean stress of the form

$$SD = a_0 + \frac{P}{a_1 + a_2 P} \tag{11}$$

where, SD is the stress difference and P is the mean stress in a triaxial compression failure test, and the parameters (a_0, a_1, a_2) are determined by a regression fit of Eq. (11) to the available laboratory data. Table 2 shows the experimentally obtained data form triaxial compression failure test for 45.6 MPa concrete. Figure 4 shows the fit to the experimental data and then predicts the failure strength.

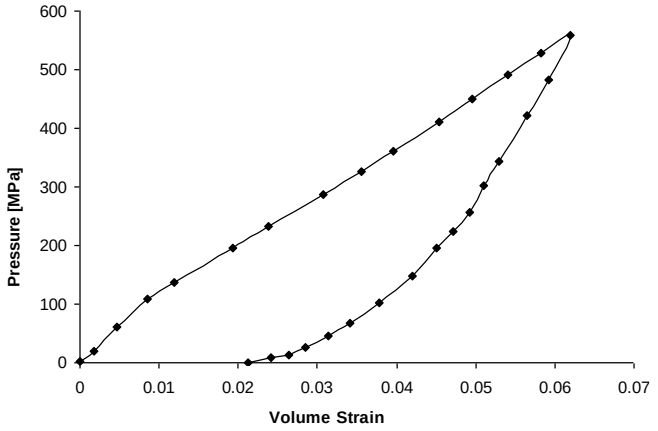

Figure 3: Pressure versus volume strain response.

Table 2: Stress difference and mean stress

Mean stress (MPa)	Stress difference (MPa)	Mean stress (MPa)	Stress difference (MPa)
0.74707	8.00122	297.332	346.943
17.1825	61.6862	342.903	382.297
38.1003	98.2235	374.28	394.818
91.1419	154.137	434.045	425.577
132.978	192.926	486.339	450.635
184.525	232.842	531.163	471.133
208.431	241.945	566.275	481.361
232.337	278.478	609.605	496.148
252.508	308.159	648.453	507.513
280.149	329.828	700.747	522.284

3.3 Determination of initial yield surface parameters, a_{oy}, a_{ly}, a_{2y}

The yield surface, the maximum failure surface and residual failure surface were determined by evaluating the parameters, namely, a_{oy}, a_{1y}, a_{2y}, a_o, a_1, a_2, a_{1f} and a_{2f}. The surface is approximately the locus of points at $\Delta\sigma = 0.45\Delta\sigma_m$ on triaxial compression paths as shown in Figure 5. For a point $(p, \Delta\sigma_m)$ on the maximum failure surface, the corresponding point $p', \Delta\sigma_y$ on the yield surface is

$$\Delta\sigma_y = 0.45\Delta\sigma_m \quad \text{and} \quad p' = p - \frac{0.55}{3}\Delta\sigma_m \tag{12}$$

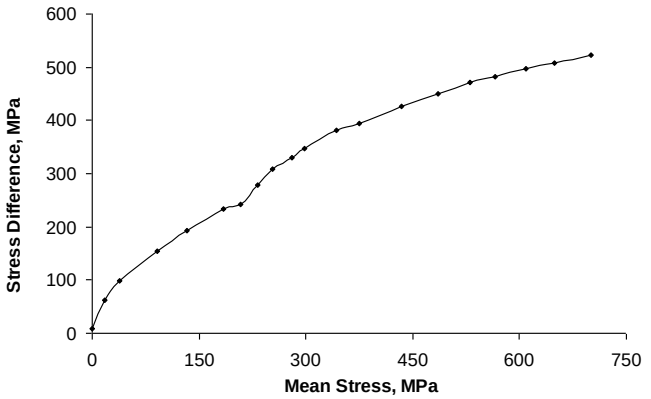

Figure 4: Triaxial compression failure surface test data.

From the later equation, p can be obtained as a function of p':

$$p = -\frac{1}{2}\left[\frac{a_1}{a_2} - p' - \frac{0.55}{3}\left(a_0 + \frac{1}{a_2}\right)\right] - \frac{1}{2}\sqrt{\left[\frac{a_1}{a_2} - p' - \frac{0.55}{3}\left(a_0 + \frac{1}{a_2}\right)\right]^2 + 4\left(\frac{0.55 a_0 a_1}{3a_2} + \frac{a_1}{a_2}p'\right)} \tag{13}$$

while the former equation gives $\Delta\sigma_y$ as a function of p is obtained from curve fitting as:

$$\Delta\sigma_y = 0.45\left(a_0 + \frac{p}{a_1 + a_2 p}\right), \tag{14}$$

enabling $\Delta\sigma_y$ to be computed as a function of p'. A plot of $\Delta\sigma_y$ is included in Figure 5. Since the proposed formulation has three parameters, the curve $\Delta\sigma_y(p')$ can be approximated by choosing three points from the curve and solving for the parameters (a_{oy}, a_{1y}, a_{2y}). By picking the first point at p'= 0, which gives ($\Delta\sigma_y = a_{0y}$), only two equations with two unknowns have to be solved for a_{1y} and a_{2y}. Table 3 shows the experimental data for determination of initial yield surface parameters.

3.4 Determination of residual failure surface parameters, a_{1f} and a_{2f}

Similar procedure as explained above can be followed to obtain the residual parameters, a_{1f} and a_{2f}. Table 4 shows the experimental data for determination of residual failure surface parameters.

Similar procedure has been followed to evaluate the parameters for concrete of strength around 60MPa [Davidson et al. (2004)].

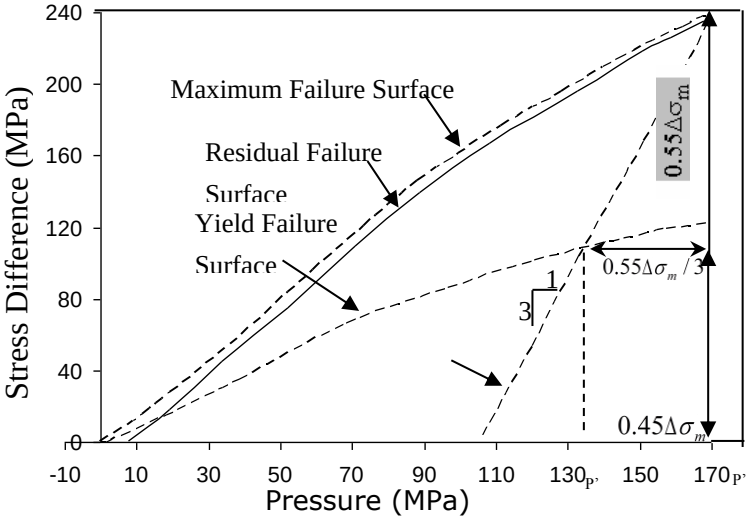

Figure 5: Yield surface determination based on triaxial compression tests

Table 3: Pressure vs Stress difference values for yield failure surface.

Pressure (MPa)	Stress Difference (MPa)
0	0
1.5	-0.74074
38.6749	34.8148
68.2714	65.9259
96.5173	85.9259
120.585	101.481
145.369	113.333
157.239	118.519
169.466	122.222

Table 4: Pressure vs Stress difference values for residual failure surface.

Pressure (MPa)	Stress Difference (MPa)
7.70821	0.818278
19.0754	18.761
33.6322	45.259
51.822	75.1673
70.4732	109.359
88.6631	139.267
108.21	167.454
132.5	196.471
150.5	218.5
158.5	226.325
167.7	235.4

4 Contact Algorithms

Several contact algorithms are available in the literature, namely, frictional sliding, single surface contact, nodes impacting on a surface, tied interfaces, one-dimensional slide lines, rigid walls, material failure along interfaces, penalty and Lagrangian projection options for constraint enforcement and fully automatic contact. Details of the typical algorithm, 'contact-automatic-single-surface' are presented below.

This algorithm uses a penalty method to model the contact interface between the different parts. In this approach, the slave and master surfaces are generated automatically within the code. The method consists of placing normal interface springs to resist interpenetration between element surfaces. An example of this approach is illustrated in Figure 6. As shown in Figure 6 , when a slave node penetrates a master surface in a time step, the code automatically detects it, and applies an internal force to the node (indicated by the spring) to resist penetration and keep the node outside the surface. The internal forces added to the slave nodes are a function of the penetrated distance and a calculated stiffness for the master surface. The stiffness is computed as a function of the bulk modulus, volume and face area of the elements in the master surface. A static and dynamic coefficient of friction of 0.8 is used between the different parts in contact.

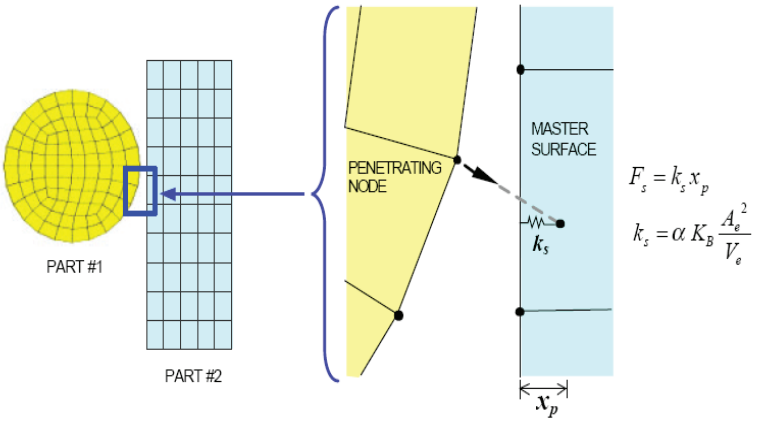

Figure 6: Penalty method for contact algorithm

5 Nonlinear Transient Explicit Finite Element Analysis

Explicit finite element method (FEM) was originally developed to solve problems in wave propagation and impact engineering, but they are currently used for many other applications such as sheet metal forming, underwater simulations, failure analysis, glass forming, metal cutting, pavement design, and earthquake engineering, among others [Benson (2001)].

Implicit FEM is expensive, when thousands of time steps must be taken to solve a dynamic problem, because of the cost of inverting stiffness matrices to solve the large sets of nonlinear equations, especially for models with thousands of degrees of freedom or when nonlinearities are present. In an explicit FEM, the solution can be achieved without forming a global stiffness matrix. The solution is obtained on an element-by-element basis and therefore, a global stiffness matrix need not be formed. As a result, explicit methods can treat large three-dimensional models (thousands of degrees of freedom) with comparatively modest computer storage requirements. Other advantages include easy implementation and accurate treatment of general nonlinearities. However, explicit methods are conditionally stable and therefore, small time steps must be used. For stable computations, the time step is selected such that the time step is less than the time required for a stress wave to travel through the shortest element and therefore, this could result in excessive execution times as the level of discretization increases.

Central-difference method, which is characteristic of explicit methods in general, for direct time integration can be used. In this method, the solution is determined in terms of historical information consisting of displacements and time derivatives

of displacements. By using this method, the finite element solution is then obtained by using the following equations (with no damping):

$$\dot{u}^{n+1/2} = \dot{u}^{n-1/2} + \Delta t.M^{-1}\left(F^{external} - \int B^T \sigma dv\right) \tag{15}$$

$$u^{n+1} = u^{n-1} + \Delta t.\dot{u}^{n+1/2} \tag{16}$$

where $F^{external}$ is the vector of applied forces associated with the boundary conditions and body forces, M is the mass matrix and $B^T \sigma dv$ is the internal force vector [15]. At each time step the velocities and displacements are updated. In general , explicit methods have the form

$$u^{n+1} = f\left(u^n, \dot{u}^n, \ddot{u}^n, u^{n-1}, \cdots\right) \tag{17}$$

and therefore, the current nodal displacements can be determined in terms of completely historical information consisting of displacements and time derivatives of displacements at previous time steps. If a diagonal mass matrix is used Eq. (17) is a system of linear algebraic equations and a solution can be obtained without solving simultaneous equations. Once displacements are updated, strains can be computed, which are then used to determine stresses and eventually nodal forces. Stable integration by using the central difference method for undamped problems requires the following time step limit:

$$\Delta t \leq \frac{L}{c_w} \tag{18}$$

where L is related to the element size and c_w is the wave speed (speed at which stress waves travel in the element). The physical interpretation of this condition for linear displacement elements is that it must be small enough, so that information does not propagate across more than one element in a time step. The shortcoming in using an explicit FEM, especially to model a quasi-static experiment is the fact that it can result in excessive execution times. Therefore, the time step will depend upon the smallest element size.

6 Performance Studies

Forrestal et al. (1994) conducted experiments to find depth of penetration with ogive nose projectiles and concrete targets with confined compressive strengths of 14, 35, 97MPa. The experimental data has been used in the present study for finite element analysis (FEA). Penetration depths are computed for various velocities by employing different material models available in NONTRANS module of FINEART. The computed penetration depth is compared with the corresponding

experimental values and LS-DYNA software. Parametric studies have been carried out by employing concrete damage model. The studies include, effect of reinforcement on penetration depth by using various options, namely, model option reinforcement, smeared model and discrete model.

The details of projectile are shown in Figure. 7. The projectile is with diameter of 1.059 in, Shank length, l_1: 8.142in, Nose edge length, l_2: 1.401in and material used is R_c (38-40) steel. The density of steel is 2.826e-4 kips/in^3 and Young's modulus is 29.36x10^{6}psi and Poisson's ratio is 0.33. The material of the target is of concrete. The target is of cylindrical shape with target diameter of 48.03in and target length of 72.05in.

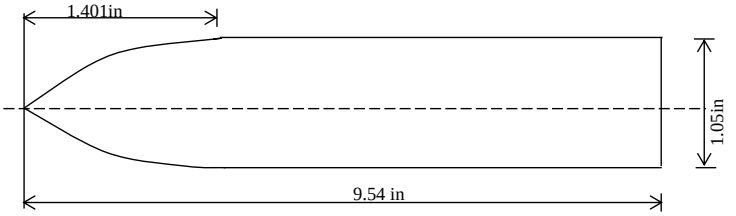

Figure 7: Projectile geometry

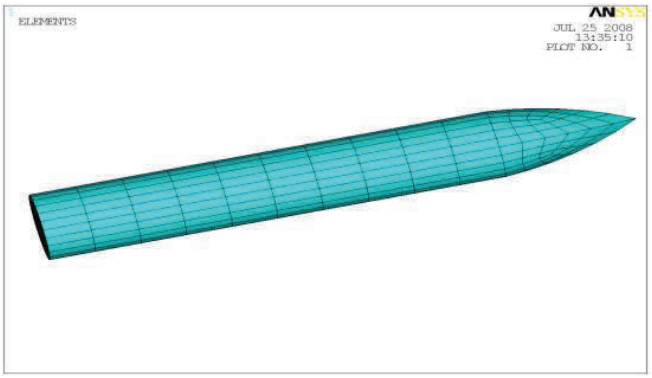

Figure 8: FE model of the projectile

Geometry and FE modeling has been carried out by using general purpose FEA software, ANSYS/LS-DYNA. Figs. 8 & 9 show the FE model of the projectile and target. Eight noded solid element has been employed to idealize the projectile and target. Each node has three degrees of freedom, namely, u_x, $u_y$and u_z. Total

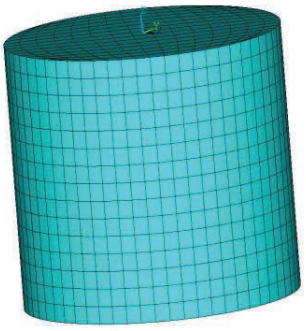

Figure 9: FE Model of the Target

Table 5: Concrete damage model

Mass density, RO	8E-5lb/in^3
Poisson's ratio, PR	0.19
Max. principal stress for failure, SIGF	450 psi
Cohesion, A_0	1478.0 psi^2
Pr. hardening coefficient, A_1	0.4463psi
Pr. hardening coefficient, A_2	0.1616e-4
Cohesion for yield, A_{0Y}	1116.0psi
Pr. hardening coefficient for yield limit, A_{1Y}	0.625
Pr. hardening coefficient for yield material, A_{2Y}	0.515e-4
Pr. hardening coefficient for jailed material, A_{1F}	0.4417
Pr. hardening coefficient for jailed material, A_{2F}	0.2366e-4
Damage scale factor, B_1	15.0
Damage scale factor for uniaxial tensile path, B_2	50.0
Damage scale factor for triaxial tensile path, B_3	0.01
% reinforcement, PER	0
Elastic modulus for reinforcement, ER	0
Poisson ratio for reinforcement, PRR	0
Initial yield stress, SIGY	0
Tangent modulus/ Plaster, ETAN	0
Load curve ID for principal material, LCP	0
Load curve ID for reinforcement, LCR	0

Table 6: Damage function coefficients

X_1 – 0	X_7 – 0.8e-4
X_2 – 0.8e-5	X_8 – 0.32e-3
X_3 – 0.24e-4	X_9 – 0.52e-3
X_4 – 0.4e-4	X_{10} – 0.57e-3
X_5 – 0.56e-4	X_{11} – 0.1e+1
X_6 – 0.72e-4	X_{12} – 0.1e+2
X_{13} – 0.1e11	
E_0 = 0, Gamma = 0, V0 = 1.0	

Table 7: Scale factor values

X_1 – 0	X_7 – 0.97
X_2 – 0.85	X_8 – 0.5
X_3 – 0.97	X_9 – 0.1
X_4 – 0.99	X_{10} – 0
X_5 – 1.0	X_{11} – 0
X_6 – 0.99	X_{12} – 0
X_{13} – 0	

Table 8: Volumetric strain data vs volumetric pressure values

ε_{v1} – 0	ε_{v6} – -3.2e-2	C_1 – 0	C_6 –0.1017e+5
ε_{v2} – -0.6e-2	ε_{v7} – -0.788e-1	C_2 – 0.325e+4	C_7 – 0.1667e+5
ε_{v3} – -1.08e-2	ε_{v8} – -3.56e-1	C_3 – 0.4973e+4	C_8 – 0.7053e+5
ε_{v4} – -1.72e-2	ε_{v9} – -0.4e+1	C_4 – 0.7086e+4	C_9 – 0.7213e+6
ε_{v5} – -2.4e-2	ε_{v10} – -0.4e+4	C_5 – 0.8906e+4	C_{10} – 0.7213e+6

Table 9: Penetration depth by using concrete damage model

Velocity (m/s)	Experimental Results (mm) (Forrestal et al. 1994)	Penetration depth (mm)	
		LS-DYNA	NONTRANS
431	411	361	377
590	729	619	648
773	866	701	813

Table 10: The revised constants for concrete damage model

a_0	1300 ps_i^2	Cohesion Constant
a_1	0.4 psi	Pressure hardening coefficient
a_2	0.15e-4	Pressure hardening coefficient
a_{0y}	1000 psi	Cohesion for Yield
a_{1y}	0.5	Pressure hardening coefficient for yield
a_{2y}	0.5e-4	Pressure hardening coefficient for yield
a_{1f}	0.4	Pressure hardening coefficient for failed material
a_{2f}	0.2e-4	Pressure hardening coefficient for failed material

Table 11: Velocity vs penetration depth by using an improved concrete damage model

Velocity (m/sec)	LS-DYNA	Penetration depth (mm)	
		Experimental (Forrestal et al. 1994)	NONTRANS
431	361 (12.16%)	411	365 (11.19%)
590	619.7 (14.99%)	729	632.1 (14.53%)
773	701.4 (19.0%)	866	765.8 (11.57%)

no. of elements in the target and projectile are 46928 and the total no. of nodes in the target and projectile are 51013. A rigid material model is employed for the projectile. Input details related to the above material models are given in Tables 5 to 8.

Contact algorithm employed between target and projectile is surface-to-surface-automatic. Input details of projectile velocity are given in Table 9. Nonlinear explicit transient dynamic analysis has been carried out by using LS-DYNA and NONTRANS. Table 9 also shows the penetration depth computed for various velocities by using LS-DYNA and NONTRANS.

Concrete damage material model has been modified with the revised constants. These constants are given as input to the material model and carried out analysis by using NONTRANS module of FINEART. Input data and the dimensions for target and projectile are same as explained above, except the values for the constants a_0, a_1, a_2, a_{0y}, a_{1y}, a_{1f} and a_{2f}. The parameters are given in Table 10.

Table 11 shows the computed penetration depth values by using an improved concrete damage model along with the corresponding values of LS-DYNA and exper-

imental studies. From Table 11, it can be observed that the computed values by using an improved concrete damage model is in good agreement with the corresponding experimental studies [Forrestal et al. (1994)].

Penetration of projectile into concrete target, variation of energy, resultant velocity and σ_{zz}- stress are shown in Figure 10 for impact velocity of 590 m/s.

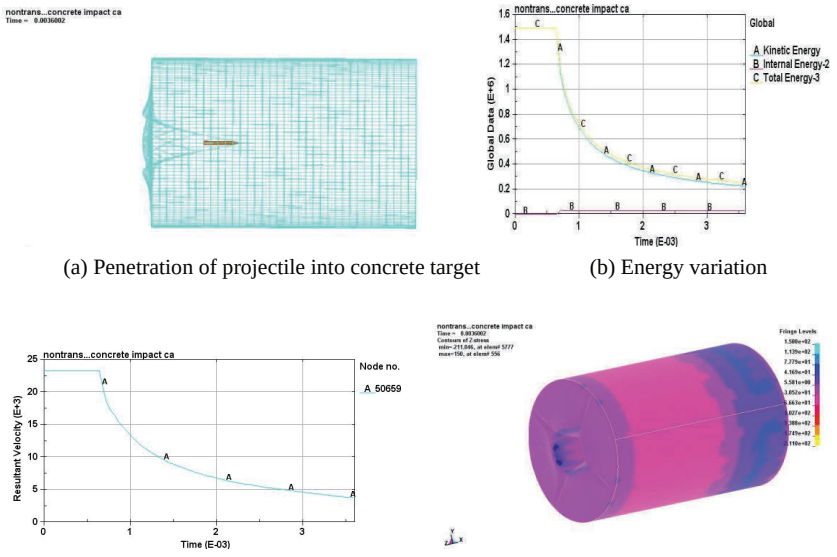

(a) Penetration of projectile into concrete target

(b) Energy variation

(c) Resultant velocity variation

(d) σ_{zz} -stress contour

Figure 10: Responses of concrete target for impact velocity of 540 m/s

7 Summary & Concluding Remarks

Nonlinear transient dynamic analysis has been carried out for simulation of projectile impact on concrete structural components by using an improved concrete damage model. The improvement is in terms of reduction of input parameters for the concrete damage model. The experimental values available in the literature have been used for evaluation of parameters. Various contact algorithms used to model the interface between the projectile and target have been discussed. The procedure for nonlinear transient explicit FEA has been presented. Based on the methodologies, program modulus have been developed and integrated with the NONTRANS module of FINEART. Numerical studies have been carried out by using FINEART and LS-DYNA software. The penetration depth is computed for different impact

velocities. The computed penetration depths obtained by using NONTRANS by employing the improved concrete damage model are in good agreement with the corresponding experimental values, whereas LS-DYNA estimates lesser value. In general, it is observed that the penetration depth increases with increase of impact velocity.

Acknowledgement: We acknowledge with thanks the valuable technical suggestions and support provided by our colleagues. This paper is being published with the permission of the Director, CSIR-SERC, Chennai, India.

References

Govindjee, S.; Kay, G. J.; Sim, J. C. (1995): Anisotropic modeling and numerical simulation of brittle damage in concrete. *Int .J. Numer. Meth. Engg.*, vol.38, pp.611–33.

Malvar, L. J.; Crawford, J. E.; Wesevich, J. W. (1997): A plasticity concrete material model for Dyna3D. *Int. J. Impact. Eng.,* vol.19, no. 9–10, pp. 847–73.

Govindjee, S.; Kay, G. J.; Simo, J. C. (1994): Anisotropic modeling and numerical simulation of brittle damage in concrete. Report Number UCB/SEM M-94/18. Berkeley, CA: University of California at Berkeley, Department of Civil Engineering.

Hentz, S.; Donze, F. V.; Daudeville, L. (2004): Discrete element modeling of concrete submitted to dynamic loading at high strain rates. *Comput Struct.,* vol. 82, no.29–30, p. 24.

Yonten, K.; Majid, T. M.; Marzougui, D.; Eskandarian, A. (2005): An assessment of constitutive models of concrete in the crashworthiness simulation of roadside safety structures. *Int. J. Crashworthiness,* vol.10, no.1, pp. 5–19.

Farnam, Y.; Soheil Mohammadi, Mohammad Shekarchi. (2010): Experimental and numerical investigations of low velocity impact behavior of high-performance fiber-reinforced cement based composite. *Int. J. Impact. Eng.,* vol.37, no.2, pp. 220-229.

Rama Chandra Murthy, A.; Palani, G. S.; Nagesh R. Iyer, Rajasankar, J.; Smitha Gopinath, Cinitha, A. (2008): State-of-the Art review on Concrete Structural Components Subjected to Impact Loading. SERC Research Report No. CSD-MLP134-RR-01.

Rama Chandra Murthy, A.; Palani, G. S.; Nagesh R. Iyer, Rajasankar, J.; Smitha Gopinath. (2009): Impact analysis of concrete structural components using empirical and analytical approaches. SERC Research Report No. CSD-

MLP134-RR-03.

AUTODYN v4.2 user manual, Century Dynamics, Inc., 2001.

LS-DYNA keyword user's manual, version 970, Livermore Software Technology Corporation; April 2003.

Schwer, L. E.; Malvar, L. J. (2005): Simplified concrete modeling with *Mat_ Concrete_Damage_Rel3. JRI LS_DYNA user week.

James, S.; Davidson, Lee Moradi.; Robert J. Dinon. (2004): Selection of a material model for simulating concrete masonry walls subjected to blast. AFRL-ML-TY-TR-2006-4521, Air force Research Laboratory.

Benson, D. (2001): A Brief Introduction to Explicit Finite Element Methods. FEA Informational News, June, pp. 2-3.

Forrestal, M. J.; Altman, B. S.; Cargile, J. D.; Hanchak, S. J. (1994): An empirical equation for penetration depth of ogive-nose projectiles into concrete targets. *Int. J. Impact. Engg.*, vol.15, no.4,

Hu, D. A.; Liang, C.; Han, X.; Chen, Y. Z.; Xu, W. F. (2012): Penetration Analysis of concrete Plate by 3D FE-SPH Adaptive Coupling Algorithm. *Comput Mater Con*, vol. 29,no.2, pp.155.